Compress Earthen Blocks using Mbam alluvial clays: Performances Comparison using Statistical Analysis of Cement versus Heat-stabilized Blocks

Christophe Enock Embom[1], Joël Fabrice Nyemb Bayamack[4], Arnaud Ngo'o Ze[1], Jacques Richard Mache[5], Jean Aimé Mbey[2*] and Vincent Laurent Onana[1,3]

[1]*Department of Earth Sciences, Faculty of Science, University of Yaoundé I, P.O. Box 812, Yaoundé, Cameroon*

[2]*Department of Inorganic Chemistry, Faculty of Science, University of Yaoundé I, P.O. Box 812, Yaoundé, Cameroon*

[3] *Department of Geosciences and Environment, University of Ebolowa, PO. 886, Ebolowa, Cameroon*

[4]*Department of Earth Sciences, Faculty of Science, University of Douala, B. P.: 24517 Douala, Cameroon*

[5]*Department of Mining Engineering, School of Mining Engineering, University of Ngaoundere, P. O Box 115, Meiganga, Cameroon*

Running head: *Cement versus heat-stabilized earthen blocks*

* Correspondence: mbey25@yahoo.fr; jean-aime.mbey@facsciences-uy1.cm

Mineralogical Society

This is a 'preproof' accepted article for Clay Minerals. This version may be subject to change during the production process.
DOI: 10.1180/clm.2024.9

Abstract

In this study, a comparison of the thermal insulating and mechanical performances of cement and heat-stabilized compressed earthen blocks (CEBs) is carried out in relation to influencing factors. The mineralogy of the used raw clays is mainly made of kaolinite, orthoclase and quartz. The mechanical strengths increase with the increase in both cement addition and firing temperature. However, the responses are higher in cement-stabilized CEBs. The thermal insulation of fired bricks is higher than that of cement-stabilized. This difference was related to the decrease in porosity and continuous surface formation. The thermal insulation decrease is mainly related to continuous surface formation in cement-stabilized CEBs, whereas for fired CEBs, it is due to the modification of pore volume. From statistical analysis, mineralogy of the raw clays combines to porosity and continuous surface development are confirmed as the main factors of both mechanical and thermal insulation modification. In cement-stabilization, the decrease insulation is due to the development of continuous surface, while for heat-stabilization, mineral transformations during the sintering reduce continuous surface formation and the insulation is controlled by both radiation and reduced surface conduction. The influence of the raw material mineralogy indicates that high clay content is favorable to the insulation in fired bricks obtained at $T \leq 1000$ °C, while high sand contents favor densification. In contrast, clay contents reduce the mechanical response of cement stabilized due to poor cement-clay interactions. In general, the mechanical response is more favorable in cement stabilization, while thermal insulation is better in fired bricks.

Key words: Kaolinite; Mineralogy; Thermal insulation; Mechanical strength; Statistical Analysis

https://doi.org/10.1180/clm.2024.9 Published online by Cambridge University Press

Introduction

The building sector still a global challenge in providing people we affordable housing of good quality. This justify the almost constant large activities in this field in both developing and so-called developed countries (Taallah *et al.*, 2014). In the past, this sector relied on the use of natural materials, including earth (Fabbri *et al.*, 2018; Elavarasan *et al.*, 2021). The earth has often been used because of its abundance, availability, low cost and energy (Gallipoli *et al.*, 2017; Hadji *et al.*, 2020).The use of earth often combined various construction techniques and standards. These include rammed earth, cob, stucco, adobe, compressed earth bricks, and terracotta (Dos Santos *et al.*, 2014; Van Damme & Houben, 2018). Unfortunately, these construction products are all sensitive to water and show limited strength. As a result, their durability is low (Elavarasan *et al.*, 2021; Benzerara *et al.*, 2021). The low durability combined with poor mastery of building techniques, as well as disputes over procedures and standards for assessing earth construction performances, have consequently led to the replacement of the earth by industrial materials. These include concrete, steel, wood, and synthetic materials (Fabbri *et al.*, 2018; Elavarasan *et al.*, 2021). However, wood construction, on the one hand, has a high environmental impact through deforestation. Concrete, steel, and synthetic constructions, on the other hand, are major indirect carbon emitters (Giada *et al.*, 2019; Benzerara *et al.*, 2021; Belarbi *et al.*, 2022). What's more, construction using these industrial materials entails significant energy consumption during operation in order to maintain thermal comfort (Giada *et al.*, 2019; Hadji *et al.*, 2020; Belarbi *et al.*, 2022). However, in the current context of sustainable development, energy supply is the key. The need for improvement is still a challenge in developing countries (Kaygusuz, 2012). In such conditions, buildings that are sustainable, ecological, and cost-effective highlight issues of material selection and processing. A return to the use of earth in the

https://doi.org/10.1180/clm.2024.9 Published online by Cambridge University Press

building industry is becoming a topic of interest for building improvement (Taallah *et al*., 2014; Fabbri *et al*., 2018; Okewale & Grobler, 2022). Indeed, earthen constructions provide much better comfort for residents through thermal insulation (Zhang *et al*., 2017). To achieve this, the need to guarantee its mechanical performance and consequently its durability is crucial (Giada *et al*., 2019; Benzerara *et al*., 2021). Numerous scientific publications were produced on improving the thermal and mechanical performances of earthen constructions. It is shown that earth-earth, earth-cement, earth-fly ash, earth-gypsum, earth-plant fibers, or even earth-geopolymer mixtures increase the mechanical performances of the resulting bricks. Thermal performances remaining similar to compress earthen block (Taallah *et al*., 2014; Zhang *et al*., 2017; Sore *et al*., 2018; Van Damme & Houben, 2018; Elavarasan *et al*., 2021; Hadji *et al*., 2020; Belarbi *et al*., 2022). In other works, it is shown that, if additives in earthen block formulation improve their mechanical performance, this is also achieved through heat treatment, which also affects the thermal performance (Bourret *et al*., 2015; Debnath *et al*., 2022). Whatever the treatment, it is obvious that the intrinsic characteristics of each soil affect the performance changes upon any given treatment. The present work aims to compare the mechanical and thermal performances of cement or heat-stabilized blocks using statistical analysis. The proposed comparison may help to identify the factors that affects the insulation behavior and/or the mechanical response of the stabilized CEB. In addition this may open route for the justification of the type of stabilized CEB to be used regarding the needed performance or the build environment in relation to the end use. The physical and thermal parameters of specimens are evaluated, as well as their mechanical responses. Statistical tools are used for a better understanding of the performance differences and the identification of the factors affecting the performances.

https://doi.org/10.1180/clm.2024.9 Published online by Cambridge University Press

1. Materials and analytical methods

1.1. Materials

Five alluvial clayey samples named MN11, MN14, MN22, BP1, and BM2 were collected along the Mbam River banks in Central Africa. This area is situated between 10°58'30''–11°20'30'' of East longitude and between 4°40'30''–5°01'15'' of North latitude. Around 70 kg of material per sample was collected in polyethylene bags for laboratory testing. Portland cement, CEM II class 42.5 R (NF EN 197-1), was used to improve the mechanical performances of raw specimens. It is a commonly used hydraulic binder in buildings. This cement is composed of around 65% Portland clinker and around 35% other constituents.

1.2. Analytical methods

1.2.1. X-ray Diffraction and X-ray Fluorescence

The mineralogical and major element compositions of the studied materials were determined by X-ray diffraction (XRD) and X-ray fluorescence (XRF), respectively. These two analytical techniques were carried out at the University of Liège, Belgium. The XRD was performed using a Bruker D8 Advance Eco diffractometer, operating with Cu-Kα radiation (λ = 1.5418 Å) under a voltage of 40 kV and a current of 30 mA. The powder XRD patternswere recorded in a 2θ range of 2 to 70° at a stepping rate of 1°/min (θ scale).The XRF was conducted on calcinated pearls, made of a 20% sample of lithium tetraborate, at 1100 °C.

1.2.2. Semi-quantitative analysis

https://doi.org/10.1180/clm.2024.9 Published online by Cambridge University Press

The mineralogical assemblage from non-oriented powder XRD was coupled to the chemical analysis of major elements for a semi-quantitative estimation using equation (1) proposed by Yvon *et al.* (1982).

$$T(x) = \sum_1^n Mi \times Pi(x) \quad (1)$$

Where *T(x)* = percentage of oxide of chemical element "x";*Mi*= percentage of mineral "i" in the sample containing chemical element "x";*Pi*(x)= proportion of element "x" oxide in mineral "i" (calculated from the ideal mineral formula of the considered mineral).

For the calculation, the following assumptions were adopted.The Fe_2O_3 is attributed to hematite or goethite;the K_2O is due to the orthoclase; the TiO_2 is solely located in rutile;the $Al_2O_3$is located in orthoclase and kaolinite; and the SiO_2 is located in orthoclase, kaolinite, and quartz.

1.2.3. Briquette elaboration, physico-mechanical and thermal characterization

Mechanical tests for flexural (σ_f) and compressive (σ_c) strengths were done on test briquettes with respective dimensions of 80 × 40 × 20 mm and 40 × 40 × 40 mm. For thermal tests, the briquettes used were of dimensions 100 × 100 × 20 mm. For the processing of those briquettes, the raw clays were oven-dried at 105°C for 24 hours, then manually ground using a porcelain mortar, and then sieved over a 1 mm mesh. All the formulations were moistened to achieve a convenient water content for molding with 8 % to 18 % water on a dry basis before being compressed using a SPECAC laboratory hydraulic press of 10 tons at a load of 1.27 MPa. In the case of clay/cement mix, the clay/cement ratios on a dry basis were 3; 6; 9; 12, and 15wt%. For the fired samples, the compressed blocks were dried at ambient at temperatures of about 27 ± 1 °C for seven days, then oven dried at 105 °C before firing at 800°C, 900°C, 1000°C, and 1100°C in an electric muffle furnace. The firing rate was of 5 °C/min. Samples are left for a 2-

https://doi.org/10.1180/clm.2024.9 Published online by Cambridge University Press

hour soak at each maximum temperature before being furnace cool down to room temperature. For clay/cement mixtures, the specimens are cured at room temperature ((27 ± 1) °C) for 28 days.

The particle size distribution of raw clays was obtained using sieving and sedimentation. Sieving is used for the coarse and fine sand fractions, respectively over 200 µm and 80 µm mesh. Robinson's pipette method is used for sedimentometry to assess the silt- and clay-sized fractions.

The dry (ρ_d) and bulk (ρ) densities of raw clays and test briquettes were determined in accordance with ASTM C373-88.

The linear shrinkage (*LS*) was determined according to the ASTM C326-03 standard. Equation (2) is used for the *LS* calculation.

$$LS\ (\%) = [(L_0 - L_1)/L_0] \times 100 \quad (2)$$

Where L_0 is the block length after compaction and L_1 is the length after firing or after room drying for 28 days.

The apparent porosity (*n*) and the water absorption (*WA*) were determined according to equations (3) and (4), respectively (ASTM C373-88).

$$n\ (\%) = [(M_2 - M_1)/(M_2 - M')] \times 100 \quad (3)$$

$$WA\ (\%) = [(M_2 - M_1)/M_1] \times 100 \quad (4)$$

Where M_1 is the specimen dry mass (g), M_2 is the specimen mass (g) after 24 hours of immersion in water, and M' is the mass of the specimen while suspended in water.

The flexural strength (σ_f) was measured in a three-point bending configuration (ASTM C674-77) on an Instron 5582 press. Flexural strength values were determined according to equation (5).

$$\sigma_f = 3PL/2lh^2 \quad (5)$$

Where P = load (N) at the breaking strength; L = distance (mm) between the two basal supports;

https://doi.org/10.1180/clm.2024.9 Published online by Cambridge University Press

l = specimen width (mm); h = specimen thickness (m).

The uni-axial compressive strength (σ_c) test was performed using an Instron servo-hydraulic press. This press has a capacity of 250 kN. The loading speed was 0.01 MPa/s.

Thermal and mechanical properties were determined on both cement-stabilized and fired specimens. The thermal effusivity (E), the specific heat capacity (ρc), the diffusivity (α), and the conductivity (λ) were determined using the asymmetric hot plate method (Bal *et al.*, 2012; Bal *et al.*, 2013). A material's thermal effusivity refers to its aptitude to exchange heat with its environment. The higher the value of E, the more the material absorbs energy from its environment (Yan & Song, 2021). α is a measure of the rate at which heat energy moves through the material. λ refers to the material's capacity to allow a heat flow to pass through it, and ρc is a property that measures the ability of a material to store heat energy. These measurements were carried out at a controlled room temperature ((20 ± 1) °C). The measurement principle involved the determination of E and ρc, assuming a unidirectional heat transfer at the center of the sample.α and λ were deduced from E and ρc according to equations (6) and (7).

$$E = \sqrt{\lambda \rho c} \quad (6)$$

$$\alpha = \lambda / \rho c \quad (7)$$

E in $JK^{-1}m^{-2}s^{-1/2}$; ρc in $JK^{-1}m^{-3}$; λ in $Wm^{-1}K^{-1}$; α in m^2s^{-1}

1.2.4. Statistical analysis

The statistical analysis was done based on the results obtained from raw materials and on 50 individuals, among whom 30 cement-stabilized CEB and 20 fired specimens. Nineteen variables were assessed. These variables included mineralogical (Qz, Kln, Hem, Gth, Ilt, and Rt), physical (Clay, silt, sand, ρ, n, WA, and LS), thermal (E, α, λ, and ρc), and mechanical (σ_f and σ_c)

https://doi.org/10.1180/clm.2024.9 Published online by Cambridge University Press

parameters. Related data were introduced in an Excel spread sheet and then analyzed using the XLSTAT version 14.5.03 software. Correlation tests were carried out to assess relationships between the 19 quantitative variables considered in pairs. The summaries of these tests are represented by correlation matrixes. The Principal Component Analysis (PCA) was also carried out with a view to assessing relationships linking the 19 quantitative variables. Data from the 30 cement-stabilized CEBs and those from the 20 fired specimens were grouped to obtain a single data set. The advantage of this statistical technique is that it synthesizes the information without truncating it. From an "n"-dimensional space defined by a "p" number of initial variables, the PCA determines a subspace of smaller dimension by searching for new variables (principal components). These new variables are often linearly independent but explain, at best, all the observations (De Lagarde, 1983). Agglomerative Hierarchical Clustering (AHC) (Ward, 1963) was executed to perform the PCA. The principle of this other technique is to construct natural groups such that specimens in the same group are similar and those in various groups are dissimilar (Bray & Curtis, 1957).

2. Results and Discussion

2.1. Raw sample physical parameters, mineral and chemical compositions

The studied materials consisted of clays (29.38–55.88%), silts (15.67–27.27%), and sands (20.04–52.59%). From the ternary diagram soil classification (Davis & Bennett, 1927), they are sandy heavy clays (MN14, MN22, BP1, and BM2) and sandy clays (MN11). Using the Winkler diagram of grain size classification, it is found that the samples are suitable for brick manufacturing (Fadil-Djenabou *et al.*, 2015; Ndjigui *et al.*, 2021). Their dry densities (ρ_d) range

https://doi.org/10.1180/clm.2024.9 Published online by Cambridge University Press

from 1.58 to 1.74 g/cm^3 (Table 1), with an average of 1.68 g/cm^3. These values are consistent with the clayey nature of the raw materials.

The XDR patterns of the raw clays are presented in Figure 1. From these patterns, the mineral assemblage is made of kaolinite, quartz, and orthoclase (K-feldspar) as the main minerals associated with hematite/goethite, rutile, and traces of anorthite and augite. The chemical composition shows main element contents for SiO_2 in the range of 55.12 % to 71.79%, Al_2O_3 in the range of 13.68 % to 20.58%, and Fe_2O_3in the range of 2.8 to 8.68%. These main elements associate TiO_2 in the range of 1.37 % to 1.58%, a content in P_2O_5< 0.09%, and total fluxes (MnO, MgO, CaO, Na_2O, and K_2O) ranging from 2.61 % to 4. 36% (Table 1).The elemental content is coherent with the mineralogical assemblage from the XRD analysis. Coupling the chemical composition with the mineralogical assemblage, a semi-quantitative evaluation of the mineral composition was done (see Section 1.2.2 for the adopted assumptions), and the obtained composition led to the following ranges: quartz 27.0–48.3 %; kaolinite 26.9–47.8%; orthoclase 8.5–16.7 %; hematite/goethite 2.8–8.6%; and rutile 1.4–1.6 % (Table 1). The kaolinite contents for all the samples are of interest for the use of these samples for construction and building materials. In addition to quartz contents, reduced swelling, shrinkage, and cracking in wet or dry states can be expected. (Gallipoli *et al.*, 2017; Van Damme & Houben, 2018). Orthoclase and flux contents, at a convenient temperature, may be favorable to the vitrification of the fired bodies from these clays.

2.2. Cement-stabilized specimens: physical, thermal, and mechanical behaviors

Bulk density values for cement-stabilized specimens vary with cement contents (Table 2). They range between 2.00 and 2.29 g/cm^3. These values fall in the range of bulk densities (1.6–2.2 g/cm^3) for cement-stabilized CEB recommended by the International Center for Earthen

https://doi.org/10.1180/clm.2024.9 Published online by Cambridge University Press

Architecture (Nshimiyimana *et al*., 2020). The cement addition induces an increase in density for all the samples. Although the clay compositions and processing are different, the density evolution observed here is similar to the reported behavior of clays from Burkina Faso by Nshimiyimana *et al.* (2020), using calcium carbide residues for stabilization. This calcium carbide, as Portland cement in hydrate mixes, leads to the formation of calcium silicate hydrate (C-S-H), which is, certainly, the main cause of the observed trend. Optimal values are achieved at 9% (dry basis) for MN14 and BM2. Slightly higher values of densities for specimens made with MN11, MN22, and BP1 are related to quartz contents, which are higher for these samples. In general, the limit value for cement addition to improve density is related to the grain size distribution and the mineralogy. For the tested samples here, it is assumed that the changes in size distribution after 9% addition of cement cause the replacement of a significant amount of larger particles, mainly associated with quartz, which has a high density. At lower contents (< 9%), the increase in density is guided by the integration of smaller cement particles within holes in the agglomerated particles of the clayey sample (Taallah *et al*., 2014).

The linear shrinkage was not measurable, indicating no shrinkage for these specimens. This trend can be associated with the presence of channels through which the excess fluid is drained with almost no displacement for the structural grains. Values of porosity (*n*) and water absorption (*WA*) in all specimens at 0 % cement and in specimens based on MN14 and BM2 materials, stabilized at 3 and 6 %, could not be determined due to the collapse of the specimens after immersion in water. The destruction in water is linked to weak cohesions between the particles of these specimens. This is caused by the high clay fraction of these samples (Taallah *et al*., 2014; Walker & Stace, 1997). In specimens in which structures were preserved, values of *n* ranged between 16.97 and 23.04 %, while *WA* ranged from 4.02 % to 10.99 % (Table 2). *WA* slightly

https://doi.org/10.1180/clm.2024.9 Published online by Cambridge University Press

increased for MN14 and BM2 samples, while it decreased for MN11, MN22, and BP1 with the increasing cement content. The porosity reduction in these specimens is linked to the progressive filling of pores by cement, which induces the decrease in *WA*. Pore filling contributes to matrix reinforcement in specimen structures and to specimen densification (Taallah *et al.*, 2014; Zhang *et al.*, 2017; Sore *et al.*, 2018). Absorbed water is generally stored in pores. As the volume of pores decreases, so does the amount of water that can be absorbed. For MN14 and BM2, *n* is almost stabilized as a result of a 9 % cement addition. This is probably due to the increased cohesion brought on by larger cement particles that agglomerate clay particles. However, the porosity of these samples (MN14 and BM2) remains higher in comparison to the others due to a coarse agglomeration that develops a loose structure within the specimens. In general, a decrease in porosity is registered while an increase in density is observed, which is in line with the observation by Zhang *et al.* (2017).

Values for thermal effusivity (E), diffusivity (α), and conductivity (λ) of cement-stabilized CEB range from $1.15\times10^{+3}$to $1.60\times10^{+3}$ $JK^{-1}m^{-2}s^{-1/2}$, 2.52×10^{-7} to 1.10×10^{-6} m^2s^{-1}, and 5.56×10^{-1} to 1.68 $Wm^{-1}K^{-1}$ respectively. The values of these parameters are minimal in specimens without added cement (0%). They increase with cement addition (Table 2) and are coherent with the density increase (Bouguerra *et al.*, 1998; Sore *et al.*, 2018). These increases reduce the thermal insulation capability of cement-stabilized specimens. The later have E values comparable to reported ones of laterite stabilized products by Meukam *et al.* (2004). Also, α and λ increase with decreasing porosity (Table 2). The higher the λ values, the more thermally conductive the material. The trends in the evolution of α and λ in the studied materials are almost similar. Indeed, the highest values of α and λ were recorded in cement-stabilized CEB, i.e., the densest, less porous CEB, where E is high. It is then obvious that cement stabilization diminished the

https://doi.org/10.1180/clm.2024.9 Published online by Cambridge University Press

insulation capacity of the blocks (Belarbi *et al.*, 2022). This decrease is related to the difference between radiation and conduction within the block. In fact, radiation occurs in the air within the pores, and it is insulating (due to its low air conductivity, $\lambda_{air} \approx 0.026$ $Wm^{-1}K^{-1b}$) (Debnath *et al.*, 2022). Conduction occurs on a solid surface, with less insulating effects, given that the conductivity of a solid is higher than that of air (Sore *et al.*, 2018; Zhang *et al.*, 2017). Given that porosity is being reduced upon cement addition, hence the amount of imprisoned air (Sore *et al.*, 2018) and consequently, the radiation capability of the material. As a reverse, the addition of cement favors solid surface development, which improves surface conduction.

Values of ρc range from $1.53\times10^{+6}$ to $2.21\times10^{+6}JK^{-1}m^{-3}$, leading to a heat mass capacity (c) range of $3440.2 \leq c \leq 4418.0$ $JK^{-1}kg^{-1}$, with the highest values in materials with 0% cement content. From these results, it is once again confirmed that the cement stabilization reduces the heat-insulating capability of the blocks as ρc values decrease with increasing cement contents in all the specimens. However, these ρc values are relatively large as compared to reported values of similar materials-based blocks from the literature (Sore *et a*l., 2018; Mansour *et al.*, 2016; Meukam *et al.*, 2004).

The flexural (σ_f) and compressive (σ_c) strengths range from 0.77 to 5.15 MPa and from 1.53 to 28.94 MPa, respectively (Table 2). The values of these two parameters increase with increasing cement contents. This trend is in line with the development of more continuous solid surfaces, as suggested by the conductivity behavior. The σ_c values of cement-stabilized CEB, as from 3% cement content, are $\geq$ 4 MPa, which indicates that these blocks are suitable in construction for load-bearing walls for two to three storey buildings in dry environments (Reeves *et al.*, 2006; Murmu & Patel, 2018; Nshimiyimana *et al.*, 2020). In specimens with 0% cement addition, only MN14 and BM2-based specimens' exhibit $\sigma_c \geq 2$ MPa, which makes them suitable

https://doi.org/10.1180/clm.2024.9 Published online by Cambridge University Press

for non-load-bearing structures for single storey buildings in dry environments. σ_f and σ_c values for MN14 and BM2 are the highest and are related to their clay contents, which are high compared to the other clayey materials. These clay mineral contents acted as a binding phase, which linked the coarse particles together in the CEB, ensuring the densification of the block (Van Damme & Houben, 2018). In cement-stabilized CEB, the cohesion between coarse particles is ensured by both the clay matrix and the cement. The hydration of cement particles leads to the formation of hydrated calcium silicate (C-S-H), which binds the coarse particles of the clayey materials, leading to a continuous surface that enhances the mechanical response (Sore *et al.*, 2018; John *et al.*, 2019). Clayey materials having moderate clay mineral contents (MN11, MN22, and BP1) exhibit a marked increase in mechanical response as from 6% cement addition. The difference between samples having higher clay mineral contents (MN14 and BM2) is due to coarse particle contents that interact with C-S-H to generate a more dense structure.

2.3. Heat-stabilized specimens: mineralogical, physical, thermal, and mechanical behaviors

The mineralogical assemblage of fired samples is made up of quartz, hematite, orthoclase, rutile, anorthite and augite. Mullite basal diffraction peak at 3.40 Å is observed as from 900 °C (Fig. 2). For samples MN14 and BM2 fired at 1100 °C, d values of ≈ 4.02 Å and ≈ 2.48 Å were associated to cristobalite. This mineralogy is coherent with that of raw materials due to the conversion of certain phases under thermal treatments. For instance, hematite is due to the conversion of goethite as from 250 °C (Ruan *et al.*, 2001; Ruan *et al.*, 2002; Gialanella *et al.*, 2010). The disappearance of kaolinite is due to its conversion into metaphase under heating as from 800 °C, which later leads to mullite crystallization and vitrification (Wang *et al.*, 2017; Lee *et al.*, 2008).

https://doi.org/10.1180/clm.2024.9 Published online by Cambridge University Press

Linear shrinkage values (*LS*) increase with the firing temperature and are relatively low (1.11% to 7.22%) (Table 3). Samples with high clay contents exhibit the highest values for *LS*. The low values of *LS* are coherent with the mineralogical assemblage of the raw materials. They are poor in fluxing agents, leading to low vitreous phase formation. Hence, the main cause of *LS* in these materials is capillary diffusion, which releases water molecules out of the structure during firing. The dehydration of oxy-hydroxide minerals such as goethite and clay minerals can constitute the main source of *LS* (He *et al*., 2012). From this, the highest values of *LS* from high clay content samples are obvious. ρ values also increase with the firing temperature. They range from 1.88 to 2.12 g/cm^3 (Table 3). These values are in line with the densities of kaolinite-based products as reported elsewhere (Pountouenchi *et al*., 2024; Njeumen *et al*., 2016). ρ values increase with increasing temperatures. This increase is related to densification, with the formation of denser phases such as mullite as from 900 °C.

Porosity (*n*) and water adsorption (*WA*) show the same trend, that is, they decrease with increasing temperature. This trend is coherent with the fact that *WA* is linked to *n*. The *n* decrease is associated with the enclosure of pores during sintering, resulting from vitreous phase formation. The values of *WA* are low, and they range from 4.12% to 7.21%. These low values indicate that all the materials are suitable for construction and building material making, as the Brazilian standard recommends *WA* < 20% (Souza *et al*., 2002; Onana *et al*., 2019).The developed porosity ranges from 17.24% to 23.75%, and it is of interest for thermal isolation (Bories *et al*., 2014). However, the firing temperature should be kept at a maximum of 1000 °C in order to benefit from the pores in thermal insulation.

The values of the thermal parameters of the fired bricks are reported in Table 3. For all the parameters, in comparison to the unfired blocks (sample dried in ambient ≈ 28 °C), they are

https://doi.org/10.1180/clm.2024.9 Published online by Cambridge University Press

decreasing in comparison to fired specimens at 800 °C. These decreases are related to kaolinite conversion into an amorphous phase upon dehydroxylation to form metakaolin, which is a less conductive phase (Bourret *et al.*, 2015). Above 800 °C, an increase in E, α, and λ is observed, resulting in a decrease in ρc. The trend change after 800 °C is associated with the crystallization and formation of phases such as mullite (Michot *et al.*, 2008), and the increase in structural organization of quartz, which is a highly conductive mineral in comparison to clay minerals (Yoon *et al.*, 2004). Hence, at low mullitization (900 °C maximum), the most conductive blocks are made of samples rich in sand (quartz) fraction, which are MN11 and MN22. At temperatures > 900 °C, the level of mullitization affects the conductivity, such that clay-rich samples (MN14 and BM2) show higher conductivity. The intermediate behavior of BP1 is driven by its clay fraction (38.06%), which is in the same range as its sand fraction (35.11%). Additionally, pore reduction upon firing also contributes to increase conductivity due to increased surface conduction.

The ranges for E, α and λ are respectively $8.67\times10^{+2}$ to $1.14\times10^{+3}$ $JK^{-1}m^{-2}s^{-1/2}$, 2.22×10^{-7} to 5.27×10^{-7} m^2s^{-1}, and 4.09×10^{-1} to 8.24×10^{-1} $Wm^{-1}K^{-1}$,while ρc values are in the range $1.55\times10^{+6}$ – $1.84\times10^{+6}$ $JK^{-1}m^{-3}$ (Table 3). These ranges of values indicate that fired bricks are more heat insulating than cement-stabilized specimens.

The values of the flexural (σ_f) and compression (σ_c) strengths are recorded in Table 3. Their respective ranges are 1.63 MPa to 6.10 MPa and 5.71 MPa to 27.83 MPa. Both strengths increase with firing temperatures as reported by others (Onana *et al.*, 2019; Roudouane *et al.*, 2020). These increases are obviously associated to the increase densification during sintering. The firing promotes vitrification and the formation of denser phases such as mullite (Buchner *et al.*, 2021; Debnath *et al.*, 2022). The role of mullite on densification is further confirmed by the highest

https://doi.org/10.1180/clm.2024.9 Published online by Cambridge University Press

strengths registered for rich clay samples MN14 and BM2. According to the Brazilian standard reported by Souza *et al.* (2002), values of $\sigma_f \geq 2$ MPa and $\sigma_f \geq 5.5$ MPa are recommended for structural brick making. Among the studied samples, MN14 and BM2 are directly suitable as from 800 °C firing, while temperatures of at least 1000 °C may be needed for the other samples unless an amendment is made to lower the temperatures.

2.4. Cement and heat-stabilized specimens: performance comparison using statistical analysis

The comparison of average values of physical parameters shows that ρ is higher in cement-stabilized CEB than in fired bricks (Table 4), whereas n is higher in fired bricks than in cement-stabilized CEB. These two parameters affected both the thermal and mechanical behaviors of the specimens. Indeed, E, α, and λ are lower in fired bricks than in cement-stabilized CEB, indicating a greater thermal insulation capacity for fired bricks. In addition, the mechanical parameters σ_f and σ_c are higher in cement-stabilized CEB than in fired bricks. The comparison of various standard deviation (SD) values (Table 4) in the two types of stabilization shows that the thermal properties (E, α, λ, and ρc) and the compressive strength (σ_c) of the studied materials are more dispersed when stabilized with cement, while the flexural strength (σ_f) dispersion is higher in fired products. These differences in dispersion globally indicated that the changes in properties are more marked in cement stabilization when compared to heat stabilization, for which there is an optimal temperature beyond which the changes are less sensitive.

Tables 5 and 6 highlight the levels of correlation between physical, mineralogical, thermal, and mechanical parameters. These tables show that ρ is moderately negatively correlated with n in both cement-stabilized and heat-stabilized materials. These negative correlations agree with the n reduction upon either firing temperature increases or cement percent increases, confirming

https://doi.org/10.1180/clm.2024.9 Published online by Cambridge University Press

the results from the measured n (see 2.2 and 2.3 sections). However, the level of correlation between ρ and n is higher (absolute value) in fired materials (R = -0.783) compared to cement-stabilized materials (R = -0.612). This is suggesting the effect of an additional factor on vitrification that is taking place in the firing process. From the correlation to linear shrinkage, LS positively correlates with ρ (R = 0.592) and negatively with n (R = -0.731) in fired specimens, the additional factor that may be considered, is the linear shrinkage. The latter affects not only the total volume of the specimen, but also the volume of voids in the specimen, resulting in the improvement of the density together with vitrification.

ρ is highly positively correlated with E, α, and λ ($R \geq 0.840$), and negatively correlated with ρc ($R \leq -0.717$). These indicate reduced insulation capacities of specimens with increasing densities and this is further confirmed by the fact that n, in contrast to ρ in the same specimens, is negatively correlated with E, α, and λ ($R \leq -0.591$), and positively with ρc ($R \geq 0.434$). Most of these correlations are high and linear (supplementary data Fig. S1a to S1i). Some of them are average in cement-stabilized specimens when compared to heat-stabilized specimens, resulting in the fact that specimens are more insulating when heat-stabilized than when cement-stabilized. The correlation to the mineralogy of cement-stabilized specimens shows that quartz and kaolinite contents are the main sources of densification. As quartz is denser than kaolinite, it is positively correlated with ρ (R = 0.456), whereas kaolinite is negatively correlated (R = -0.492). This negative correlation to kaolinite is probably associated with the poor interaction that may be generated between the clay and the fine cement particles. This poor interaction may not be favorable to densification. In contrast, interactions with more coarse quartz particles induce an increase in densification. Correlations of the density with raw sample mineralogy in fired specimens are not relevant, as the changes in mineral forms of clays to mullite or quartz to its

https://doi.org/10.1180/clm.2024.9 Published online by Cambridge University Press

allomorphs (such as cristobalite) should be considered. The same applies to their thermal parameters (Table 6). It is then postulated that the less insulating behavior of the cement-stabilized CEB is due to pore organization defaults that favor surface conduction, in contrast to heat-stabilized specimens, in which the mineralogical conversion of the clay mineral and vitrification generate control pore structures in which radiation in the imprisoned air is developed. However, the mechanical responses of the fired specimens are favorably correlated to kaolinite contents ($R \geq 0.695$), as a result of their conversion during sintering in more dense phases such as mullite. *LS* and the clay fraction, in heat stabilization, are positively linearly correlated with mechanical strengths (supplementary data Fig. S1k to S1n). This is not the case in cement-stabilized CEB since there is almost no shrinkage.

Correlations between thermal (E, α, and λ) and mechanical parameters (σ_f and σ_c) are positive and significant ($R \geq 0.702$) in cement-stabilized materials (Table 5), whereas for heat-stabilized materials, correlations are positive but less significant ($R \leq 0.526$) (Table 6). The structure of the specimens is probably the main cause of the differences. In cement stabilized, the formation of calcium silicate hydrate (C-S-H) favors continuous surface formations, which improve mechanical responses but reduce insulation capacities as the surface conduction is improved. In fired products, the sintering process implies the vitreous phase's formation. In the latter, non-modified mineral grains are embedded together with the partial mineral conversion of some phases. This leads to less continuous surfaces that contribute to enhance insulation due to the lowering of surface conduction.

From the PCA, the cumulated percentage of variance (56.79) presented by the two axes F1 and F2 is not too high to make a good component analysis. To avoid misinterpretation of the graphic, the F1–F3 factorial plan has been added, for a cumulated percentage of variance of 71.09

https://doi.org/10.1180/clm.2024.9 Published online by Cambridge University Press

(supplementary dataTable S1). Results relative to the contribution of variables for the construction of these axes show that thirteen parameters are well expressed. This contribution is supported by the square cosine method (supplementary data Table S2). According to this method, clay, sand, Qz, Kln, ρ, n, α, and λ on the F1 axis, σ_f and σ_c on the F2 axis, and silt, Hem, and Rt on the F3 axis are well represented and reflect reality. An interpretation based on silt, ρ, n, WA, E, Gth, and Or would be secondary.

In the F1–F2 correlation circle (Fig. 3a), Kln and clay are positively correlated. These two variables are negatively correlated with Qz and sand. E, α, λ, ρ, σ_f, and σ_c are close, i.e., positively correlated among them. These correlations corroborate observations made upwards, i.e., the higher the ρ values, the higher the E, α, λ, σ_f, and σ_c values. In the F1–F3 factorial plan (Fig. 3b), sand and Qz are close to ρ, α, and λ. This group of parameters is almost significantly negatively correlated with clay, Kln, and n. These other correlations reaffirm the incidence of the mineralogical variety on the density and, consequently, on the thermal performances. The resulting clouds of individuals (Fig. 3c and 3d) show that the F1 axis almost separates cement-stabilized CEB from heat-stabilized specimens. This is highlighting the effect of the two stabilization techniques on the initial materials. These two groups can however be redistributed into three classes. Indeed, the AHC organizes the studied cement and heat-stabilized materials into classes 1, 2, and 3 (Fig. 4).The class 1 groups both cement (10 individuals) and heat (17 individuals) stabilized CEB. This class is governed by moderate to high clay, sand, quartz, and kaolinite contents (clay = 38.16%, sand = 41.97%, Qz = 40.71%, and Kln = 35.75%) (supplementary data Table S3). Specimens in this class show good mechanical performances when cement-stabilized. They show good insulation capabilities and moderate to good mechanical performances when heat-stabilized. Class 2 (07 individuals) only consists of cement-

https://doi.org/10.1180/clm.2024.9 Published online by Cambridge University Press

stabilized CEB and the governing factors here are high clay and kaolinite, and moderate sand and quartz contents (clay = 49.42%, Kln = 44.92%, sand = 25.27%, and Qz = 28.88%). Specimens in this class are marked by high insulation capacities and low mechanical performances. Class 3, as class 1, is also composed of both cement (13 individuals) and heat (03 individuals) stabilized CEB. Here the governing factors are high clay and kaolinite, and moderate sand and quartz contents (clay = 48.56%, Kln = 44.26%, sand = 28.15%, and Qz = 30.51%). Specimens in this class show, whatever the stabilization type, moderate to high insulation capacities and moderate mechanical performances.

Conclusion

Clayey materials from the Mbam River banks were characterized and used for earthen building blocks making. The aim was to evaluate their thermal and mechanical performances after cement and heat stabilization. These materials consist of kaolinite, orthoclase and quartz as main minerals, with hematite, goethite, rutile, anorthite, and augite as associate minerals. Their densities are coherent with their nature as soil materials, with variations associated with differences in mineral phase contents, mainly kaolinite and quartz. Overall, the thermal insulation of the studied materials is good, with better performances for heat-stabilized, especially fired specimens below 1000 °C. The insulation capacity of heat-stabilized specimens reduces with temperature increase as a result of pore reduction. However, the poor development of continuous surfaces allows the thermal insulation to remain higher when compared to cement-stabilized specimens. It is shown that cement-stabilized specimens show greater mechanical responses than heat-stabilized specimens. Around 9% cement addition is the ideal level for cement-stabilized specimens, particularly for those rich in kaolinite. While for firing, a minimum of 900 °C should

https://doi.org/10.1180/clm.2024.9 Published online by Cambridge University Press

be recommended to obtain suitable fired bricks. It was established using statistics that the mineralogy of raw samples determines the insulation behavior of the stabilized CEB. For fired samples, high clay content favor the insulation behavior through the transformation of clay minerals from the starting materials. Discontinuities arising from clay minerals conversion and the vitreous phase formation induce reduced conduction surfaces, which favor the thermal insulating performances. *LS* was found to be an additional factor for porosity changes in heat stabilization. For cement stabilized, the role of C-S-H in continuous surface development was proposed as main course of thermal insulation reduction. High clay content is not favorable to the mechanical response in cement-stabilization due to poor clay-cement interaction. Coarse particles, such as sand, are need to ensure good cohesion and interaction between the C-S-H and the fine fraction due to clay.

Overall, although the starting material mineralogy should be considered, in relation to the needed performances, the mechanical responses are of more interest with cement stabilization while thermal insulation is better using firing.

Acknowledgements:

The Cameroonian Minister of Higher Education is acknowledge for the special research allowance to the research staff in the state Universities.

Funding: This research did not receive any specific grant from funding agencies in the public, commercial, or not-for-profit sectors

Competing Interests: The authors declare that they have no known competing financial interests or personal relationships that could have appeared to influence the work reported in this paper.

References

Bal H., Jannot Y., Quenette N., Chenu A. & Gaye S. (2012)Water content dependence of the porosity, density and thermal capacity of laterite based bricks with millet waste additive. *Construction and Building Materials*, **31**, 144–150.

Bal H., Jannot Y., Gaye S. & Demeurie F. (2013) Measurement and modelisation of the thermal conductivity of a wet composite porous medium: Laterite based bricks with millet waste additive. *Construction and Building Materials*, **41**, 586–593.

Belarbi Y.E., Sawadogo M., Poullain P., Issaadi N., Hamami A.E.A., Bonnet S. & Belarbi R. (2022) Experimental Characterization of Raw Earth Properties for Modeling Their Hygrothermal Behavior. *Buildings*, **12**, 648. https://doi.org/10.3390/buildings12050648

Davis R.O.E. & Bennett H.H. (1927) *Grouping of Soils on the Basis of Mechanical Analysis*, Department circular 419, U.S. Department of Agriculture, Washington, D. C., 15p.

Benzerara M., Guihéneuf S., Belouettar R. & Perrot A. (2021) Combined and synergic effect of algerian natural fibres and biopolymers on the reinforcement of extruded raw earth. *Construction and Building Materials*, **289**, 123211. https://doi.org/10.1016/j.conbuildmat.2021.123211

Bories C., Borredon M.-E., Verdrenne E. &Vilarem G. (2014) Development of eco-friendly porous fired clay bricks using pore-forming agents: A review. *Journal of Environmental Management*, **143**, 186–196. http://dx.doi.org/10.1016/j.jenvman.2014.05.006b

Bouguerra A., Diop M.B., Laurent J.P., Benmalek M.L.& Queneudec M. (1998) Effect ofmoisture content on the thermal effusivity of wood cement-based composites. *Journal of Physics D: Applied Physics*, **31**, 3457. DOI: 10.1088/0022-3727/31/24/008

Bourret J., Tessier-Doyen N., Guinebretiere R., Joussein E. & Smith D.S. (2015) Anisotropy of thermal conductivity and elastic properties of extruded clay-based materials: Evolution with thermal treatment. *Applied Clay Science*, **116–117**, 150–157.

Bray J.B. & Curtis J.T. (1957) An ordination of the upland forest communities of Southern Wisconsin. *Ecological Monographs*, **27**, 326–349.

https://doi.org/10.1180/clm.2024.9 Published online by Cambridge University Press

Buchner T., Kiefer T., Königsberger M., Jäger A. & Füssl J. (2021) Continuum micromechanics model for fired clay bricks: Up scaling of experimentally identified microstructural features to macroscopic elastic stiffness and thermal conductivity. *Materials & Design*, **212**, 110212. https://doi.org/10.1016/j.matdes.2021.110212

De Lagarde J. (1983) *Initiation à l'Analyse des Données*. Dunod, Paris, 3ème édition, 157 pp.

Debnath N.K., Pabbisetty V.K., Sarkar K., Singh A., Majhi M.R. & Singh V.K. (2022) Preparation and characterization of semi-silica insulation refractory by utilizing lignite fly ash waste materials. *Construction and Building Materials*, **345**, 128321. https://doi.org/10.1016/j.conbuildmat.2022.128321

Dos Santos C.A., Librelotto L.I. & Jacintho C., (2014) Building with earth – Brazil's most popular raw earth building techniques and the opinion of experienced builders. *Key Engineering Materials*, **600**, 123–131.

Elavarasan S., Priya A.K., Raja Gurusamy R., Mohamed Riyas Naveeth J. & Natesh, S., (2021) Experimental study on compressed earth block using fly-ash stabilizer. *Materials Today: Proceedings*, **37**, 3597 – 3600. https://doi.org/10.1016/j.matpr.2020.09.641

Fabbri A., Morel J-C., Gallipoli D., (2018) Assessing the performance of earth building materials: a review of recent developments. *RILEM Technical Letters*, **3**, 46–58.

Fadil-Djenabou S., Ndjigui P-D. & Mbey J.A. (2015) Mineralogical and physicochemical characterization of Ngaye alluvial clays (Northern Cameroon) and assessment of its suitability in ceramic production. *Journal of Asian Ceramic Societies*, **3**, 50–58, http://dx.doi.org/10.1016/j.jascer.2014.10.008

Gallipoli D., Bruno A.W., Perlot C. & Mendes J.(2017)A geotechnical perspective of raw earth building. *Acta Geotechnica*, **12**, 463–478.

Giada G., Caponetto R. & Nocera F. (2019) Hygrothermal Properties of Raw Earth Materials: A Literature Review. *Sustainability*, **11**, 5342. https://doi.org/10.3390/su11195342.

https://doi.org/10.1180/clm.2024.9 Published online by Cambridge University Press

Gialanella S., Girardi F., Ischia G., Lonardelli I., Mattarelli M. & Montagna M. (2010) On the goethite to hematite phase transformation. *Journal of Thermal Analysis and Calorimetry*, **102**, 867–873.

Hadji F., Ihaddadene N., Ihaddadene R., Betga A., Charick A. & Logerais P.O. (2020) Thermal conductivity of two kinds of earthen building materials formerly used in Algeria. *Journal of Building Engineering*, **32**, 101823. https://doi.org/10.1016/j.jobe.2020.101823

He H., Yue Q., Su Y., Gao B., Gao Y., Wang J. & Yu H. (2012) Preparation and mechanism of the sintered bricks produced from Yellow River silt and red mud. *Journal of Hazardous Materials*, **203**, 53–61.

John E., Epping J.D. & Stephan D. (2019) The influence of the chemical and physical properties of C-S-H seeds on their potential to accelerate cement hydration. *Construction and Building Materials*, **228**, 116723. https://doi.org/10.1016/j.conbuildmat.2019.116723

Kaygusuz K. (2012) Energy for sustainable development: A case of developing countries. *Renewable and sustainable energy reviews*, **16**, 1116–1126.

Lee W.E., Souza G.P., McConville C.J., Tarvornpanich T. & Iqbal Y.(2008) Mullite formation in clays and clay-derived vitreous ceramics. *Journal of the European Ceramic Society*, **28**, 465–471.

Mansour M., Jelidi A., Cherif A. & Jabrallah S. (2016) Optimizing thermal and mechanical performance of compressed earth blocks (CEB). *Construction and Building Materials*, **104**, 44–51.

Meukam P., Jannot Y., Noumowe A. & Kofane T.C. (2004) Thermo physical characteristics of economical building materials. *Construction and Building Materials*, **18**,437–443.

Michot A., Smith D.S., Degot S. & Gault C. (2008) Thermal conductivity and specific heat of kaolinite: Evolution with thermal treatment. *Journal of the European Ceramic Society*, **28**, 2639–2644.

https://doi.org/10.1180/clm.2024.9 Published online by Cambridge University Press

Murmu A. L. & Patel A. (2018) Towards sustainable bricks production: An overview. *Construction and Building Materials*, **165**, 112–125.

Ndjigui P-D, Mbey J. A., Fadil-Djenabou S., Onana V.L., Bayiga E.C., Enock Embom C. & Ekosse G-I. (2021) Characteristics of Kaolinitic Raw Materials from the Lokoundje River (Kribi, Cameroon) for Ceramic Applications. *Applied Sciences*, **11**, 6118. https://doi.org/10.3390/app11136118.

Njeumen Nkayem D. E., Mbey J.A., Kenne Diffo B.B. & Njopwouo D. (2016) Preliminary study on the use of corn cob as pore forming agent in lightweight clay bricks: Physical and mechanical features. *Journal of Building Engineering*, **5**, 254-259. http://dx.doi.org/10.1016/j.jobe.2016.01.006

Nshimiyimana P., Fagel N., Messan A., Wetshondo D. O. & Courard L. (2020) Physico-chemical and mineralogical characterization of clay materials suitable for production of stabilized compressed earth blocks. *Construction and Building Materials*, **241**, 118097. https://doi.org/10.1016/j.conbuildmat.2020.118097

Okewale A. I. & Grobler H. (2022) Investigations into suitability of tropical clay for engineering applications. *Innovative Infrastructure Solutions*, **7**, 85. https://doi.org/10.1007/s41062-021-00683-x

Onana V.L., Ntouala R.F.D., Mbey J.A., Ngo'o Ze A., Kabeyene V.K. & Ekodeck G.E. (2019) Mineralogy and preliminary assessment of the potential uses of alluvial clays from Batouri (Eastern-Cameroon). *Cerâmica,* **65**, 407–415. http://dx.doi.org/10.1590/0366-69132019653752626

Pountouenchi A., Njoya A., Mbey J.A., Mache J.R., Njoya D., Yongue F. R., Njopwouo D., Fagel N., Pilate P. & Van Parys L. (2023) Characterization of refractory bricks from selected Cameroonian kaolins. *Clay Minerals*, https://doi.org/10.1180/clm.2023.32

Reeves G.M., Sims I. & Cripps J.C., editors (2006) *Clay Materials Used In Construction*. Geological Society of London, Engineering Geology Special Publications, **21**, 513 pp.

https://doi.org/10.1180/clm.2024.9 Published online by Cambridge University Press

Ruan H.D., Frost R.L. & Kloprogge J.T. (2001) The behavior of hydroxyl units of synthetic goethite and its dehydroxylated product hematite. *Spectrochimica Acta Part A: Molecular and Biomolecular Spectroscopy*, 57, 2575–2586.

Ruan H.D., Frost R.L., Kloprogge J.T. & Duong L. (2002) Infrared spectroscopy of goethite dehydroxylation: III. FT-IR microscopy of in situ study of the thermal transformation of goethite to hematite. *SpectrochimicaActa Part A: Molecular and Biomolecular Spectroscopy*, **58**, 967–981.

Roudouane H. T., Mbey J. A., Bayiga E. C. & Ndjigui P-D. (2020) Characterization and application tests of kaolinite clays from Aboudeia (southeastern chad) in fired bricks making, *Scientific African*, **7**, e00294, https://doi.org/10.1016/j.sciaf.2020.e00294

Sore S.O., Messan A., Prud'homme E., Escadeillas G. & Tsobnang F. (2018) Stabilization of compressed earth blocks (CEBs) by geopolymer binder based on local materials from Burkina Faso. *Construction and Building Materials*, **165**, 333–345.

Souza G.P., Sanchez R. & De Hollanda J.N.F. (2002) Characteristics and physical-mechanical properties of fired kaolinitic materials. *Cerâmica*, **48**, 102–107.

Taallah B., Guettala A., Guettala S. & Kriker A. (2014) Mechanical properties and hygroscopicity behavior of compressed earth block filled by date palm fibers. *Construction and Building Materials*, **59**, 161–168.

Van Damme H. & Houben H. (2018) Earth concrete. Stabilization revisited. *Cement and Concrete Research*, **114**, 90–102.

Walker P. & Stace T. (1997) Properties of some cement stabilised compressed earth blocks and mortars. *Materials and structures*, **30**, 545-551.

Wang G., Wang H. & Zhang N. (2017) In situ high temperature X-ray diffraction study of illite. *Applied Clay Science*, **146**, 254–263.

Ward J.H. (1963) Hierarchical grouping to optimize and objective function. *Journal of the American statistical association*, **58**, 236–44.

https://doi.org/10.1180/clm.2024.9 Published online by Cambridge University Press

Yan Y.K. & Song Y.F. (2021) Research on application and thermal performance of raw earth material in building envelope. *Journal of Physics: Conference Series*, 1777, 012041. DOI 10.1088/1742-6596/1777/1/012041.

Yoon Y.-G., Car R., Srolovitz D.J. &Scandolo S. (2004) Thermal conductivity of crystalline quartz from classical simulations. *Physical Review B*, **70**, 012302. https://link.aps.org/doi/10.1103/PhysRevB.70.012302

Yvon J., Lietard O. & Cases J.M. (1982) Minéralogie des argiles kaoliniques des Charentes. *Bulletin de Mineralogie*, **105**, 431–437.

Zhang L., Gustavsen A., Jelle B.P., Yang L., Gao T. & WangY. (2017) Thermal conductivity of cement stabilized earth blocks. *Construction and Building Materials*, **151**, 504–511.

https://doi.org/10.1180/clm.2024.9 Published online by Cambridge University Press

Table 1. Physical parameters, mineralogical and chemical compositions of the raw materials

Parameters	MN11	MN14	MN22	BP1	BM2
Clay	29.38	55.88	39.31	38.06	52.69
Silt	18.03	20.83	15.67	26.83	27.27
Sand	52.59	23.29	45.02	35.11	20.04
Sum	100	100	100	100	100
Dry density (g/cm^3)	1.74	1.68	1.70	1.71	1.58
Quartz	48.3	27.0	44.2	30.1	29.3
Kaolinite	26.9	47.8	37.6	40.6	45.8
Hematite	2.8	-	-	-	6.8
Goethite	-	8.6	4.5	7.1	-
Orthoclase	16.7	9.1	8.5	15.4	11.0
Rutile	1.5	1.4	1.5	1.6	1.6
Anorthite	ε	ε	ε	ε	ε
Augite	ε	-	ε	ε	ε
SiO_2	71.59	55.12	67.24	59.04	57.71
Al_2O_3	13.68	20.58	16.43	18.9	20.13
Fe_2O_3	2.8	8.68	4.53	7.15	6.83
MnO	0.03	0.04	0.02	0.03	0.06
MgO	0.29	0.71	0.33	0.82	1.01
CaO	0.55	0.44	0.52	0.51	0.63
Na_2O	0.36	0.36	0.28	0.39	0.02
K_2O	2.82	1.54	1.44	2.61	1.86
TiO_2	1.5	1.37	1.48	1.58	1.57
P_2O_5	0.05	0.04	0.04	0.05	0.08

This is a 'preproof' accepted article for Clay Minerals. This version may be subject to change during the production process.
DOI: 10.1180/clm.2024.9

LOI	5.61	11.58	7.67	8.74	10.43

ε: traces

https://doi.org/10.1180/clm.2024.9 Published online by Cambridge University Press

Table 2. Physical, thermal and mechanical characteristics of cement-stabilized specimens

Sample	Cement content (%)	ρ (g/cm^3)	n (%)	WA (%)	E (J/K m^2 s$^{1/2}$) $\times 10^3$	α (m2/s) $\times 10^{-7}$	λ (W/mK) $\times 10^{-1}$	ρc (J/K m^3) $\times 10^6$	σ_f (Mpa)	σ_c (Mpa)
MN11	0	2.04	-	-	1.23	4.90	8.62	1.76	0.77	1.53
	3	2.14	20.68	6.14	1.38	6.64	11.29	1.70	1.39	4.03
	6	2.16	19.35	5.29	1.50	8.16	13.52	1.66	2.68	12.70
	9	2.20	17.92	4.28	1.54	8.78	14.40	1.64	4.51	21.91
	12	2.23	17.23	4.18	1.56	9.98	15.54	1.56	4.66	23.40
	15	2.25	16.97	4.02	1.60	11.00	16.78	1.53	4.83	25.80
MN14	0	2.00	-	-	1.20	2.93	6.48	2.21	1.35	2.77
	3	2.02	-	-	1.34	4.30	8.80	2.05	1.83	4.76
	6	2.09	-	-	1.36	5.24	9.81	1.87	2.92	10.17
	9	2.12	22.85	6.97	1.38	5.75	10.49	1.82	3.90	16.63
	12	2.10	22.91	8.01	1.32	5.23	9.55	1.83	4.12	17.22
	15	2.05	23.04	10.99	1.26	4.77	8.73	1.83	4.20	19.78
MN22	0	2.07	-	-	1.15	3.83	7.09	1.85	0.85	1.89
	3	2.16	20.99	6.90	1.33	5.17	9.56	1.85	1.78	5.24
	6	2.19	19.91	5.04	1.40	6.34	11.14	1.76	3.27	14.79
	9	2.22	19.01	4.63	1.51	7.74	13.30	1.72	3.91	25.79
	12	2.25	18.44	4.39	1.54	8.15	13.94	1.71	4.63	27.71
	15	2.29	17.70	4.23	1.58	8.67	14.74	1.70	5.15	28.94
BP1	0	2.09	-	-	1.22	3.50	7.22	2.07	0.87	1.98
	3	2.18	20.62	6.07	1.37	4.78	9.49	1.99	1.43	5.28
	6	2.20	19.74	5.77	1.49	6.57	12.05	1.83	2.76	12.82
	9	2.23	18.87	4.52	1.54	7.05	12.91	1.83	3.74	21.43
	12	2.24	18.49	4.43	1.53	7.05	12.88	1.83	4.17	24.34
	15	2.25	18.07	4.34	1.55	7.27	13.24	1.82	4.19	25.73
BM2	0	2.01	-	-	1.17	2.98	6.38	2.14	1.30	2.36
	3	2.05	-	-	1.35	4.44	8.98	2.02	1.76	5.07

	6	2.08	-	-	1.47	5.41	10.83	2.00	3.05	9.18
	9	2.14	22.08	5.45	1.49	6.10	11.66	1.91	3.98	15.17
	12	2.10	22.53	7.21	1.34	4.89	9.38	1.92	4.01	17.91
	15	2.07	22.78	8.76	1.29	4.49	8.63	1.92	4.05	18.59

https://doi.org/10.1180/clm.2024.9 Published online by Cambridge University Press

Table 3. Physical, thermal and mechanical characteristics of heat-stabilized specimens

Sample	Temperature (°C)	ρ (g/cm^3)	n (%)	WA (%)	LS (%)	E (J/K m^2 s$^{1/2}$) $\times 10^2$	α (m^2/s) $\times 10^{-7}$	λ (W/mK) $\times 10^{-1}$	ρc (J/K m^3) $\times 10^6$	σ_f (Mpa)	σ_c (Mpa)
MN11	800	1.94	20.20	6.52	1.11	9.59	3.02	5.27	1.75	1.63	5.71
	900	1.95	20.06	6.18	1.50	9.71	3.51	5.75	1.64	1.66	6.82
	1000	1.99	20.01	5.69	1.71	9.86	3.86	6.12	1.59	1.73	6.98
	1100	2.03	19.98	5.42	1.80	10.76	4.83	7.48	1.55	1.84	7.80
MN14	800	1.88	23.75	6.24	1.37	8.67	2.22	4.09	1.84	2.92	11.21
	900	1.96	21.81	6.01	2.24	9.11	2.49	4.54	1.83	4.15	17.81
	1000	2.02	19.55	5.66	3.74	11.06	4.33	7.28	1.68	4.88	24.83
	1100	2.12	17.24	4.12	7.22	11.35	5.27	8.24	1.56	6.10	27.83
MN22	800	1.97	21.39	6.43	1.30	9.82	3.05	5.43	1.78	1.74	7.65
	900	2.03	20.89	6.06	1.64	10.31	3.64	6.22	1.71	1.88	7.97
	1000	2.07	20.48	5.88	1.84	10.62	4.17	6.86	1.65	2.09	8.79
	1100	2.10	19.57	5.63	2.25	10.81	4.47	7.23	1.62	2.69	10.44
BP1	800	1.91	21.84	6.07	1.20	9.23	2.90	4.97	1.72	1.65	6.75
	900	1.93	20.57	5.92	1.52	9.43	3.05	5.21	1.71	1.75	7.44
	1000	1.99	19.65	5.79	1.78	10.41	3.87	6.47	1.67	1.92	7.85
	1100	2.02	19.32	4.97	1.93	10.55	4.31	6.93	1.61	2.36	8.90
BM2	800	1.87	22.30	7.21	1.35	9.19	2.56	4.65	1.82	2.64	11.07
	900	1.93	21.37	6.27	2.05	9.64	2.94	5.23	1.78	4.31	16.34
	1000	1.96	19.95	6.14	3.63	1097	4.06	6.99	1.72	5.66	21.34
	1100	2.05	17.72	4.58	5.35	11.39	4.76	7.86	1.65	5.73	24.32

https://doi.org/10.1180/clm.2024.9 Published online by Cambridge University Press

Table 4. Statistical summaries of measured variables in cement and heat stabilized CEB

Stabilization	Statistics	ρ	n	WA	LS	$E\times10^{3}$	$\alpha\times10^{-7}$	$\lambda\times10^{-1}$	$\rho c\times10^{6}$	σ_f	σ_c
Cement	Minimum	2	16.97	4.02	0	1.15	2.93	6.38	1.53	0.77	1.53
	Maximum	2.29	23.04	10.99	0	1.60	11.0	16.8	2.21	5.15	28.94
	Average	2.14	20.01	5.79	0	1.40	6.07	10.9	1.84	3.07	14.16
	SD	0.08	1.7	1.51	0	0.13	2.01	2.76	0.16	1.39	9.09
Firing	Minimum	1.87	17.24	4.12	1.11	0.87	2.22	4.09	1.55	1.63	5.71
	Maximum	2.12	23.75	7.21	7.22	1.14	5.27	8.24	1.84	6.1	27.83
	Average	1.99	20.38	5.84	2.33	1.01	3.67	6.14	1.69	2.97	12.39
	SD	0.07	1.49	0.69	1.55	0.08	0.86	1.19	0.087	1.56	7.02

SD: Standard Deviation

https://doi.org/10.1180/clm.2024.9 Published online by Cambridge University Press

Table 5. Correlation matrix of variable in cement-stabilized CEB

Variables	Clay	Silt	Sand	Qz	Kln	Hem	Gth	Or	Rt	*ρ*	*n*	*WA*	*LS*	*E*	*α*	*λ*	*ρc*	σf	σc
Clay	**1**																		
Silt	**0,393**	**1**																	
Sand	**-0,939**	**-0,685**	**1**																
Qz	**-0,818**	**-0,763**	**0,933**	**1**															
Kln	**0,940**	**0,533**	**-0,944**	**-0,916**	**1**														
Hem	0,208	**0,442**	-0,330	-0,080	0,054	**1**													
Gth	0,332	0,015	-0,269	**-0,504**	**0,504**	**-0,817**	**1**												
Or	**-0,707**	0,236	**0,471**	0,292	**-0,647**	0,107	-0,326	**1**											
Rt	-0,356	**0,580**	0,065	0,029	-0,185	**0,473**	**-0,484**	**0,511**	**1**										
ρ	**-0,630**	-0,233	**0,586**	**0,456**	**-0,492**	-0,328	-0,010	0,330	0,291	**1**									
n	**0,665**	0,277	**-0,630**	**-0,535**	**0,599**	0,210	0,154	**-0,425**	-0,235	**-0,612**	**1**								
WA	**0,575**	0,177	**-0,522**	**-0,453**	**0,498**	0,113	0,190	-0,359	-0,319	**-0,598**	**0,873**	**1**							
LS																			
E	**-0,444**	-0,096	**0,388**	0,319	**-0,388**	-0,079	-0,140	0,338	0,242	**0,875**	**-0,591**	**-0,601**		**1**					
α	**-0,641**	**-0,392**	**0,654**	**0,617**	**-0,664**	-0,119	-0,268	**0,408**	0,094	**0,856**	**-0,653**	**-0,571**		**0,896**	**1**				
λ	**-0,587**	-0,294	**0,575**	**0,524**	**-0,579**	-0,113	-0,223	**0,390**	0,153	**0,889**	**-0,648**	**-0,598**		**0,956**	**0,986**	**1**			
ρc	**0,688**	**0,595**	**-0,768**	**-0,756**	**0,756**	0,188	0,277	-0,348	0,059	**-0,717**	**0,434**	0,324		**-0,654**	**-0,885**	**-0,825**	**1**		
σf	-0,019	-0,087	0,048	0,070	-0,038	-0,006	-0,029	-0,043	-0,041	**0,637**	-0,187	-0,125		**0,732**	**0,702**	**0,732**	**-0,572**	**1**	
σc	-0,190	-0,145	0,205	0,176	-0,153	-0,142	0,017	0,037	0,038	**0,760**	-0,342	-0,255		**0,777**	**0,761**	**0,790**	**-0,629**	**0,957**	**1**

Values in bold are different from 0 with a level of signification alpha = 0.05

https://doi.org/10.1180/clm.2024.9 Published online by Cambridge University Press

Table 6. Correlation matrix of variables in heat-stabilized specimens

Variables	Clay	Silt	Sand	Qz	Kln	Hem	Gth	Or	Rt	ρ	n	WA	LS	E	α	λ	ρc	σ_f	σ_c
Clay	**1**																		
Silt	0,393	**1**																	
Sand	**-0,939**	**-0,685**	**1**																
Qz	**-0,759**	-0,341	**0,729**	**1**															
Kln	**0,940**	**0,533**	**-0,944**	**-0,903**	**1**														
Hem	0,208	0,442	-0,330	0,190	0,054	**1**													
Gth	0,332	0,015	-0,269	**-0,609**	**0,504**	**-0,817**	**1**												
Or	**-0,707**	0,236	**0,471**	**0,745**	**-0,647**	0,107	-0,326	**1**											
Rt	-0,356	**0,580**	0,065	0,124	-0,185	**0,473**	**-0,484**	**0,511**	**1**										
ρ	-0,063	-0,397	0,198	-0,071	-0,073	-0,282	0,139	-0,261	-0,252	**1**									
n	0,084	-0,020	-0,059	-0,117	0,094	-0,063	0,093	-0,119	-0,067	**-0,783**	**1**								
WA	-0,110	-0,045	0,104	0,105	-0,135	0,196	-0,271	0,019	0,171	**-0,778**	**0,805**	**1**							
LS	**0,550**	0,165	**-0,498**	-0,314	**0,468**	0,149	0,137	-0,352	-0,288	**0,597**	**-0,731**	**-0,764**	**1**						
E	0,072	-0,065	-0,032	-0,092	0,052	0,074	-0,073	-0,178	-0,001	**0,840**	**-0,868**	**-0,717**	**0,706**	**1**					
α	-0,092	-0,134	0,123	0,081	-0,112	-0,018	-0,063	-0,004	-0,026	**0,881**	**-0,892**	**-0,807**	**0,665**	**0,951**	**1**				
λ	-0,017	-0,103	0,052	0,005	-0,038	0,020	-0,063	-0,080	-0,020	**0,874**	**-0,893**	**-0,783**	**0,697**	**0,983**	**0,992**	**1**			
ρc	**0,453**	0,213	-0,438	-0,384	0,441	0,143	0,106	-0,343	-0,074	**-0,760**	**0,783**	**0,723**	-0,382	**-0,714**	**-0,883**	**-0,822**	**1**		
σf	**0,817**	0,343	**-0,775**	**-0,470**	**0,701**	0,370	0,074	**-0,500**	-0,270	0,284	-0,420	**-0,469**	**0,861**	**0,496**	0,362	0,428	0,007	**1**	
σc	**0,810**	0,280	**-0,746**	**-0,473**	**0,695**	0,268	0,161	**-0,516**	-0,361	0,336	**-0,455**	**-0,506**	**0,890**	**0,526**	0,401	**0,464**	-0,038	**0,981**	**1**

Values in bold are different from 0 with a level of signification alpha = 0.05

https://doi.org/10.1180/clm.2024.9 Published online by Cambridge University Press

Figures and Captions

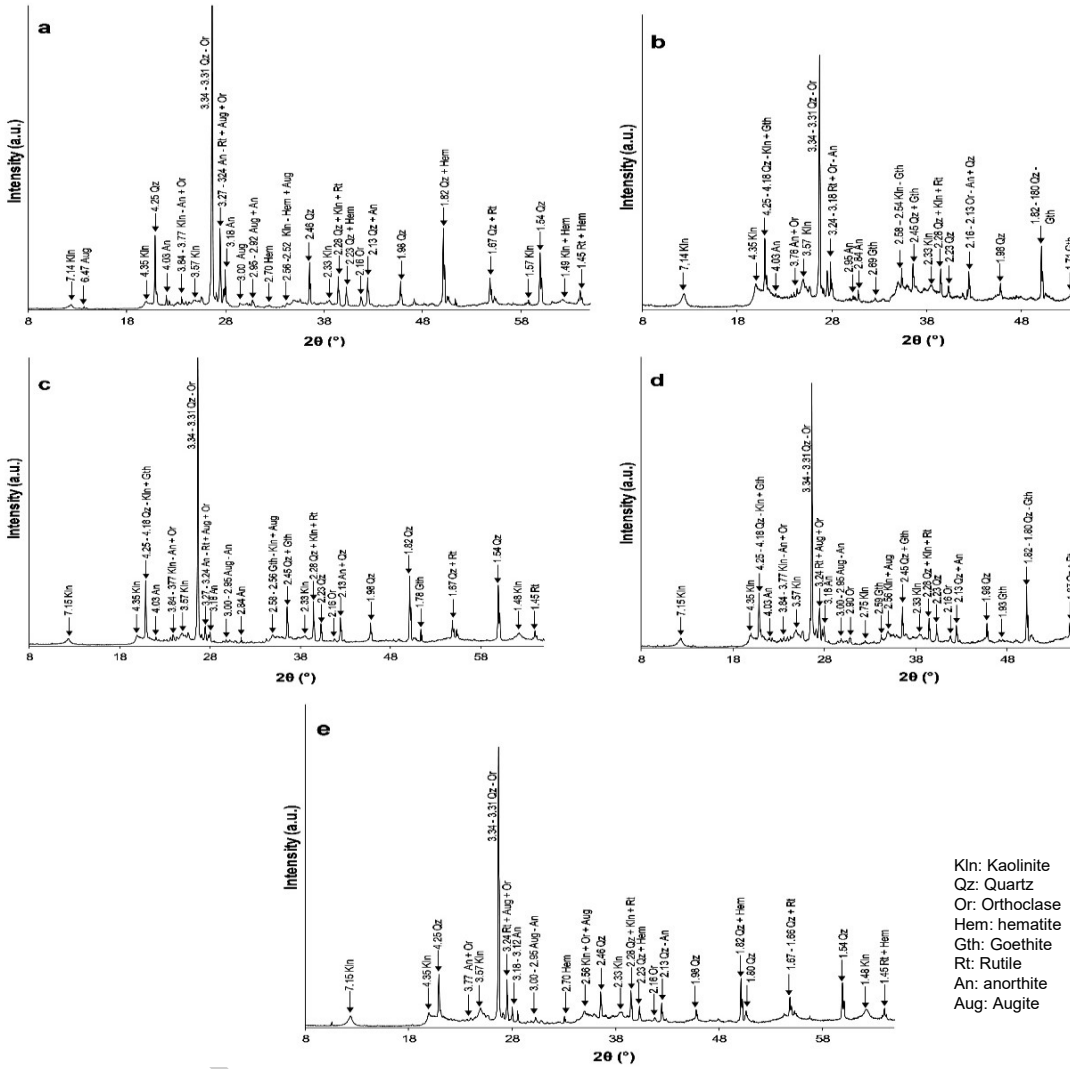

Note:The numbers indicate the d in Å associted to the diffraction peak

Fig.1. XRD patterns of raw materials. (a) MN11. (b) MN14. (c) MN22. (d) BP1. (e) BM2

Mineralogical Society

This is a 'preproof' accepted article for Clay Minerals. This version may be subject to change during the production process.
DOI: 10.1180/clm.2024.9

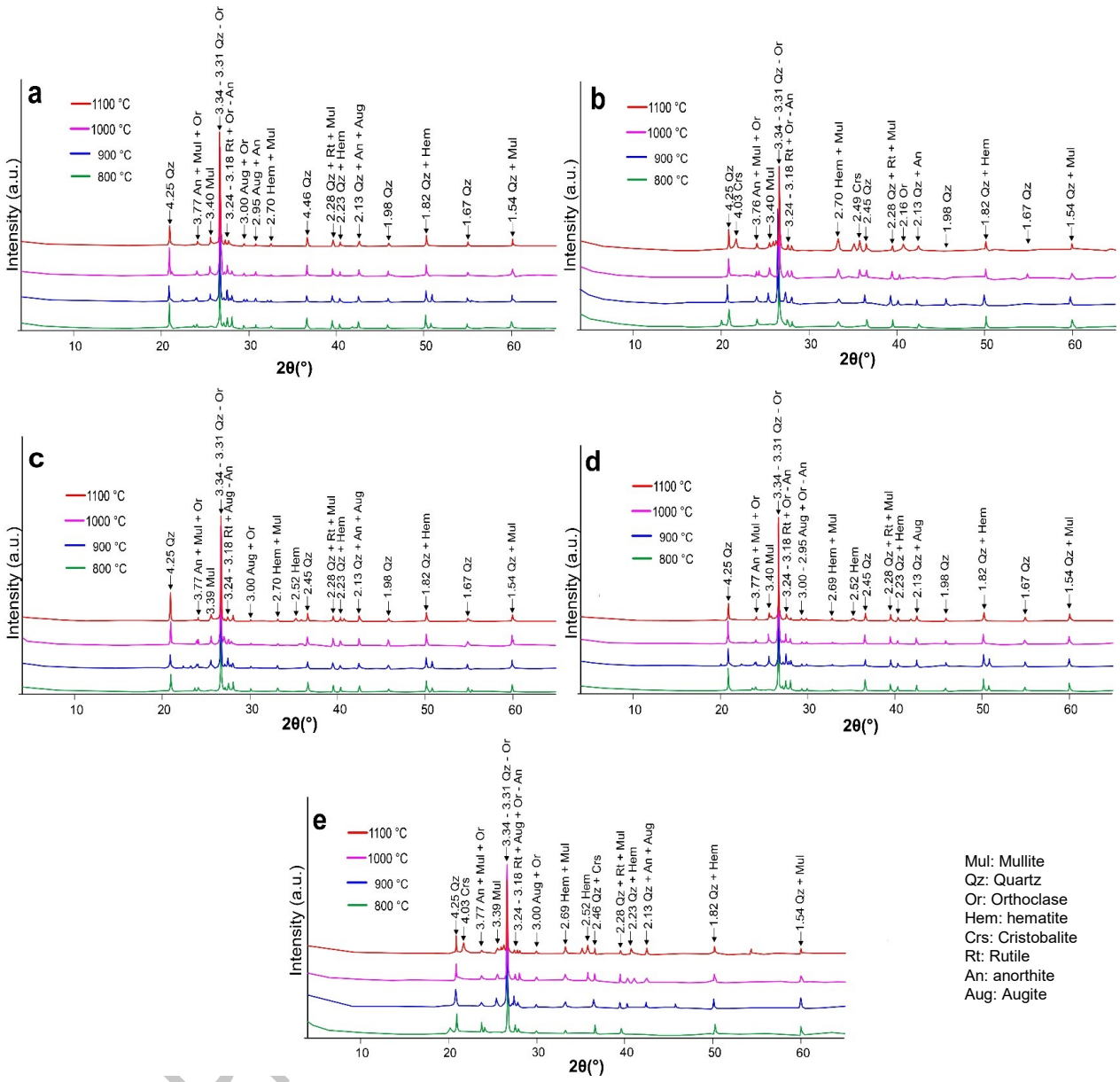

Fig. 2. XRD patterns of fired briquettes. (a) MN11. (b) MN14. (c) MN22. (d) BP1. (e) BM2

https://doi.org/10.1180/clm.2024.9 Published online by Cambridge University Press

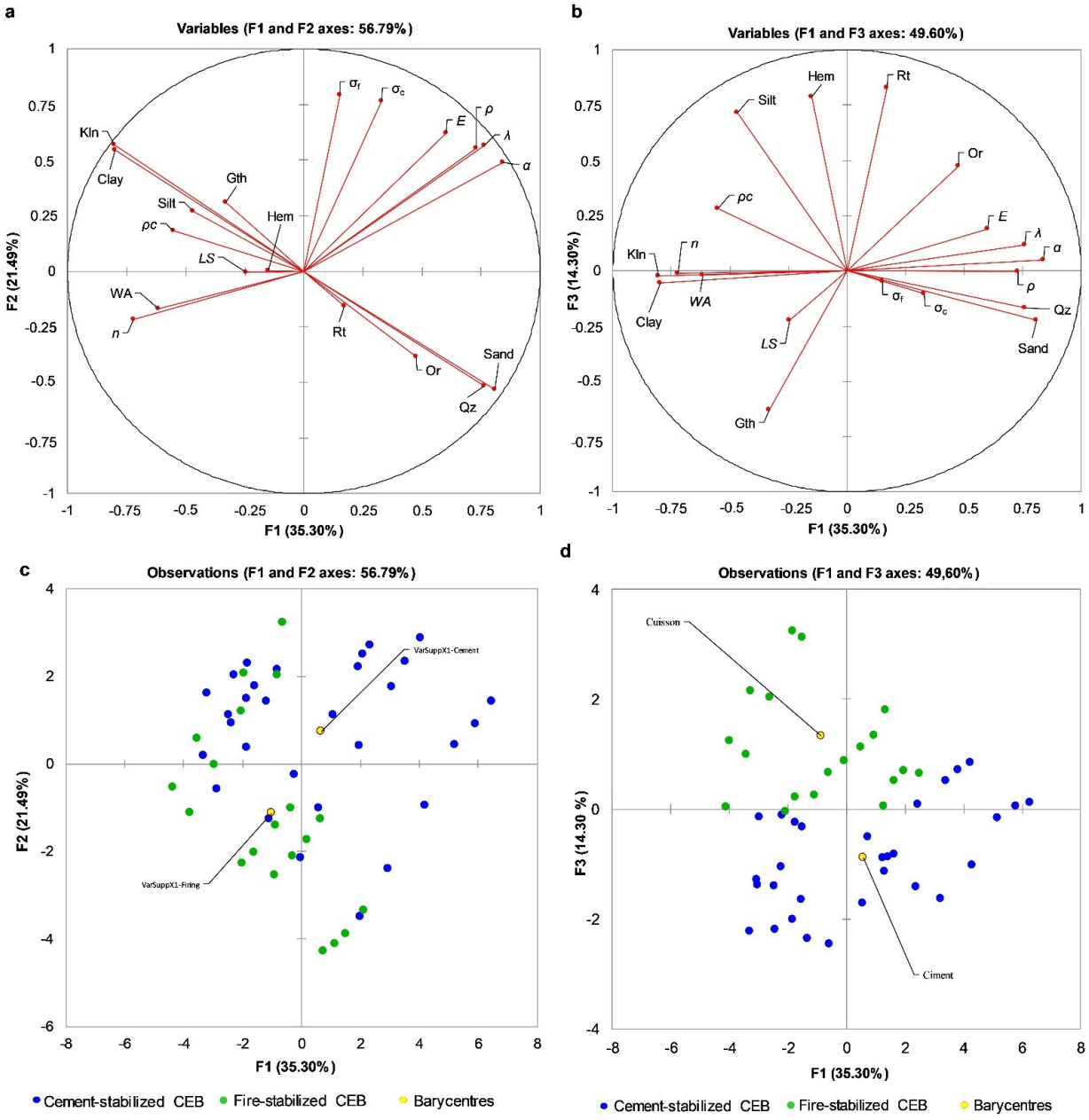

Fig. 3. PCA of variables (a and b) and individuals of cement and heat stabilized CEB

https://doi.org/10.1180/clm.2024.9 Published online by Cambridge University Press

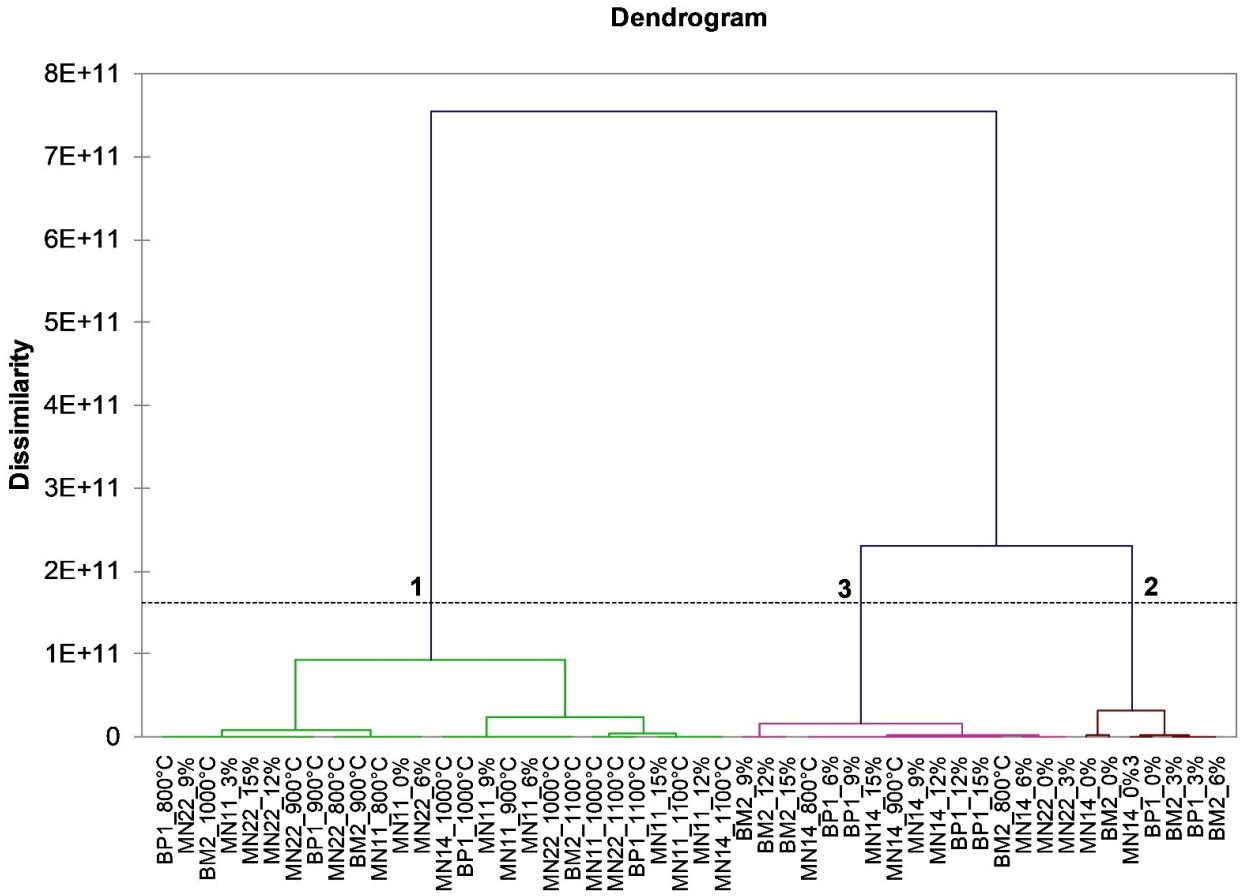

Fig. 4. Dendrogram of cement and heat stabilized materials

https://doi.org/10.1180/clm.2024.9 Published online by Cambridge University Press